

Estimation of the Vertical Land Motion from GNSS Time Series and Application in Quantifying Sea-Level Rise

J.-P. Montillet, M.S. Bos, T.I. Melbourne, S. D. P. Williams, R. M. Fernandes, W.M. Szeliga

Abstract Sea-level rise observed at tide gauges need to be corrected for vertical land motion, observed with GNSS, to obtain the absolute sea-level rise with respect to the centre of the Earth. Both the sea-level and vertical position time series contain temporal correlated noise that need to be taken into account to obtain the most accurate rate estimates and to ensure realistic uncertainties. Satellite altimetry directly observes absolute sea-level rise but these time series also exhibit coloured noise. In this chapter we present noise models for these geodetic time series such as the commonly used first order Auto Regressive (AR), the General Gauss Markov (GGM) and the ARFIMA model. The theory is applied to GNSS and tide gauge data from the Pacific Northwest coast.

J.-P. Montillet

Space & Earth Geodetic Analysis Laboratory, Universidade da Beira Interior, Portugal
- Institute of Earth Surface Dynamics, University of Lausanne, Lausanne, Switzerland
e-mail: jpmontillet@segal.ubi.pt

M.S. Bos

Instituto D. Luís, Universidade da Beira Interior, Portugal e-mail: machiel@segal.ubi.pt

T.I. Melbourne

Pacific Northwest Geodetic Array laboratory, Central Washington University, Ellensburg, Washington state, USA e-mail: tim@geology.cwu.edu

S. D. P. Williams

Marine Physics and Ocean Climate group, National Oceanography Centre, Liverpool, UK e-mail: sdwil@noc.ac.uk

R.Fernandes

Instituto D. Luís, Universidade da Beira Interior, Portugal e-mail: rui@segal.ubi.pt

W. M. Szeliga

Pacific Northwest Geodetic Array laboratory, Central Washington University, Ellensburg, Washington state, USA e-mail: walter@geology.cwu.edu

1 Introduction

One of the greatest consequences of climate change is rising the sea level. Due to thermal expansion, the sea level is expected to increase by a third of a meter by 2100. The exchange of water between the continents and the oceans has the potential to cause as much as two meters of sea-level change by 2100, mainly due to the melting of ice on the land and the subsequent oceanic runoff. Greenland and Antarctica contain enough ice to raise global mean sea-level by 7 m and 55 m respectively. Therefore, even the melting of only a fraction of those large ice sheets can cause significant sea-level rise. Mountain glaciers and other ice fields contain another meter of potential sea-level change. According to recent studies (*Church and White, 2011; IPCC, 2013*), sea-level rise will not be uniform around the world, due to spatial variations in ocean density and due to change in gravity and ocean floor deformation associated with the redistribution of this extra mass of water. Some ocean regions might even see sea-level fall but on average sea-level is expected to rise significantly in response to climate change. The melting of large bodies of ice causes distinct patterns or fingerprints in the regional distribution of sea-level change (*Davis et al., 2012*).

Regional sea-level can be monitored with tide gauges. However, these instruments only measure the relative sea-level and the vertical land motion at the tide gauges needs to be observed to convert the relative sea-level observations into absolute ones (*Church et al., 2010*). If these tide gauge records are used to make historical reconstructions of global sea-level rise, then the uncertainty in the spatial covariance is another source of error (*Christiansen et al., 2010*). As a result, careful modelling has to be applied before processing tide gauge data taking into account stochastic processes and the correction with vertical land motion.

Stochastic processes in tide gauge data are generally defined as temporal correlated noises which can affect the estimation of the rate uncertainty rather than the estimated rate, also called relative sea-level rise (*Montillet et al., 2018*). Temporal correlations are known to exist in many different types of climatological and geophysical time-series (*Press, 1978; Agnew, 1992; Beran, 1992*). Temporally correlated noise means that each observation is not completely independent of the previous observations and effectively provides less information than an independent or non-correlated observation. Several models have been used to model those correlations (*Church and White, 2011*), including a fifth-order auto regressive (*Hughes and Williams, 2010; Hay et al., 2013*). However, *Agnew (1992)* pointed out that the power spectral density (PSD) of sea-level variations may be better described by a power-law stochastic model. This stochastic model is generally described as a coloured noise. The coloured noise can be defined in the frequency domain as a $1/f^\alpha$ noise, with α varying between $[0, 2]$. When the exponent of the coloured noise is set to 0, the noise is called white noise, at 1 it is defined as Flicker noise,

whereas at 2 it corresponds to a random-walk. More details can be found in Chapter 2 of this book.

Along the coast, a combination of various geophysical processes generates the vertical land motion (VLM) either regionally or locally near the tide gauge. The nature of these geophysical processes can be from natural or anthropogenic origins, creating linear or transient non-linear signals. In particular, the study of long tide gauge (TG) records are impacted by glacial isostatic adjustment (GIA) due to late Pleistocene deglaciation and interseismic tectonic strain accumulation without local earthquakes (*Lambeck and Johnston, 1995; Mitrovica and Davis, 1995*). Non-linear processes include earthquakes, annual hydrological oscillations either stationary or non-stationary in amplitude or phase, time-dependent anthropogenic aquifer depletion or other resource extraction signals, soil compaction, climatic and ocean loading signals. These signals must be taken into account when studying local and regional sea-level rise due to the same order of magnitude (mm/yr) (*Bos et al., 2014; Hamlington et al., 2016; Montillet et al., 2018*).

Fortunately, precise vertical land motion rates relative to the Earth's reference frame can be estimated due to the availability of a dense network of GPS stations generating a coastal profile. It then provides local and regional corrections of solid-Earth processes that could potentially bias sea-level rise measurements. Furthermore, this smooth regional VLM profile around the coast resulting from the vast number of permanently installed coastal GPS stations (e.g., *Meertens et al., 2015; Blewitt et al., 2016*), can be used by climate scientists studying regional and global variations of the sea-level rise, without requiring any GPS expert knowledge.

In the next section, we will discuss functional and stochastic noise models involved in an accurate estimation of relative sea-level rise (SLR) from tide gauges, and in particular the correction with vertical land motion (VLM) using near-by GNSS stations in order to obtain an absolute SLR. Section 3 is an application of this methodology in the estimation of sea-level rise in the pacific northwest (USA). This example shows how to model GNSS time series and tide gauges in order to produce reliable estimates. We emphasize the various sources of error. The last section is a general discussion on the estimation of global mean sea-level with the current research topics.

2 Estimation of Sea-Level Rise

2.1 Relative sea-level observed with tide gauges

The oldest measuring technique to observe the sea level has been tide gauges. These have been installed in almost any harbour around the world to, as the name implies, observe the local tides to ensure the safe entering and leaving

of ships. The earliest tide gauges were nothing more than a marked staff in the water that was read at regular intervals. The float tide gauge was an improvement together with the automatic recording of the sea level on paper rolls that made it possible to produce very long and accurate time series such as those observed in Honolulu, Hawaii, (*Colosi et al.*, 2006) and Boston, USA, (*Talke et al.*, 2018).

The Permanent Service for Mean Sea Level (PSMSL) has been collecting monthly and yearly sea level data from tide gauges around the world (*Holgate et al.*, 2013) and this data set has been used in many sea level studies. The trajectory model that is fitted to the observations is in most cases a simple linear trend plus an annual and semi-annual signal although a tri-annual signal is needed in some cases as well. *Church et al.* (2004) used simple weighted least-squares and a simple first order autoregressive noise model, AR(1), which is defined as:

$$w_i = \phi w_{i-1} + v_i \quad (1)$$

where w_i is the noise in the time series at time t_i , ϕ a constant between -1 and 1 and v_i a Gaussian random variable. *Bos et al.* (2014) have verified that this works well for yearly data but not so much for monthly data. The reason is that the AR(1) only needs to represent the noise for periods of 2 to around 100 years. When monthly data is used, then this increases from 2 months to 100 years and AR(1) has trouble to correctly describe the stochastic properties for this wider frequency range.

In Chapter 2, we rewrote Eq. (1) in terms of a filter \mathbf{h} that was applied to the vector \mathbf{v} with Gaussian random variables:

$$w_i = \sum_{j=0}^i h_j v_{i-j} \quad (2)$$

For the AR(1) noise model we have $h_0 = 1$ and $h_1 = \phi$. In matrix notation this becomes:

$$\mathbf{w} = \begin{pmatrix} h_0 & 0 & \dots & 0 \\ h_1 & h_0 & & 0 \\ \vdots & & \ddots & \vdots \\ h_{N-1} & \dots & h_1 & h_0 \end{pmatrix} \mathbf{v} = \mathbf{L} \mathbf{v} \quad (3)$$

Here \mathbf{L} is a lower triangle matrix (only values on and below the diagonal) and it is Toeplitz. The covariance matrix \mathbf{C} is equal to $\sigma^2 \mathbf{L} \mathbf{L}^T$. *Langbein* (2017) demonstrates that the inverse of matrix \mathbf{L} is again a lower triangle matrix and also Toeplitz:

$$\mathbf{L}^{-1} = \begin{pmatrix} h'_0 & 0 & \dots & 0 \\ h'_1 & h'_0 & & 0 \\ \vdots & & \ddots & \vdots \\ h'_{N-1} & \dots & h'_1 & h'_0 \end{pmatrix} \quad (4)$$

The new elements h'_i of the inverse of matrix \mathbf{L} can be computed as follows:

$$\begin{aligned} h'_0 &= 1/h_0 && \text{for } i = 0 \\ h'_i &= -1/h_0 \sum_{j=0}^{i-1} h'_j h_{i-j} && \text{for } i > 1 \end{aligned} \quad (5)$$

Note that $h_0 = 1$. Therefore, if the standard deviation of the Gaussian variable \mathbf{v} is σ , then the logarithm of the determinant of the covariance matrix \mathbf{C} is $2N \ln \sigma$. Furthermore, if \mathbf{A} and \mathbf{y} are the design matrix and the vector containing the observations, then it is convenient to define the following variables:

$$\begin{aligned} \mathbf{B} &= \frac{1}{\sigma} \mathbf{L}^{-1} \mathbf{A} \\ \mathbf{z} &= \frac{1}{\sigma} \mathbf{L}^{-1} \mathbf{y} \end{aligned} \quad (6)$$

The weighted least-squares estimation now becomes:

$$\mathbf{x} = \left(\mathbf{B}^T \mathbf{B} \right)^{-1} \mathbf{B}^T \mathbf{y} \quad (7)$$

Introducing residuals $\mathbf{r} = \mathbf{z} - \mathbf{B}\mathbf{x}$, the log-likelihood function can be written as:

$$\ln(L) = -\frac{1}{2} \left[N \ln(2\pi) + 2N \ln \sigma + \mathbf{r}^T \mathbf{r} \right] \quad (8)$$

By choosing the values for the parameters of the noise model, the coefficients h_i can be computed. Together with the noise amplitude σ , the covariance can be constructed which, using Eqs. (5) to (7) can be used to fit the trajectory model using weighted least-squares. These noise parameters and the noise amplitude must vary until the maximum log-likelihood value, Eq. (8), has been found. This maximum likelihood scheme has been implemented in the Hector software (*Bos et al.*, 2013). Figure 1 shows the monthly sea level of the tide gauge at Seattle which is one of the gauges discussed in section 3. Using Eqs. (4) to (8), a linear trend plus annual and semi-annual signal has been fitted to the observations which is also shown in Figure 1. The power spectral density of the residuals is plotted in Figure 2 together with the fitted noise model AR(1). Eq. (1) can be extended to be dependent on the last five noise values which is called a fifth order autoregressive model, AR(5). This is also shown in Figure 2 together with the Generalised Gauss Markov

Fig. 1: Monthly tide gauge data from Seattle (source PSMSL) with the fitted trajectory model.

Fig. 2: Power spectral density plot of the residuals for the Seattle monthly tide gauge data. Fitted are the power spectra using an AR(1), AR(5) and GGM noise model.

noise model of *Langbein* (2004). The latter noise model fits better to the observed power spectra at the lowest frequencies. Other possible noise models are ARMA and ARIMA which work well for time series with short-term correlations. On the other hand the FARIMA model is more suited in the presence of long-term correlations due to the versatility of modeling coloured noise and other non-stationary stochastic processes (e.g., *Panas*, 2001; *Montillet and Yu*, 2014). Studies, such as *Bos et al.* (2014), estimate optimally the lags p and q in the ARMA(p,q), ARIMA(p,d,q) and the FARIMA(p,d,q) models using information criteria (e.g., Akaike Information Criterion or AIC (*Akaike*, 1974) or the Bayesian Criterion (BIC) (*Schwarz*, 1978)) following *Burnham and Anderson* (2002). AIC and BIC are defined as follows:

$$\begin{aligned} AIC &= -2\ln(L) + 2k \\ BIC &= -2\ln(L) + k\ln(N) \end{aligned} \tag{9}$$

Thus, they are -2 times the log-likelihood plus a penalty term. The penalty term corrects for the fact that a more flexible noise model will in most cases fit the observed power spectrum better. By using a penalty term the more flexible model will only be chosen if this model is significantly better. Due to the minus sign of $-2\ln(L)$, the best model is the one that has the lowest AIC or BIC value. Note that the parameter d in the ARIMA model is an integer value (in $\mathbb{Z}, d > 0$), whereas it is a real (in $\mathbb{R}, d > 0$) in the FARIMA model. These noise models are explained in more detail in Chapter 2. *Bos et al.* (2014) demonstrated that sea level observations show weaker power-law noise at the very low frequencies compared to GNSS data. As a result, the effect on the uncertainty of the estimated linear trend, compared to a simple white noise model, is less than that for GNSS time series.

Besides linear sea-level rise, there have been various studies that estimate sea-level acceleration using tide gauge data (*Jevrejeva et al.*, 2008) and satellite altimetry (*Church and White*, 2006; *Yi et al.*, 2017; *Nerem et al.*, 2018). It is the acceleration which is mainly responsible for the large sea-level rise of 0.3-1 m mentioned in the introduction at the end of this century. To estimate this acceleration, the first order polynomial in the trajectory model is replaced by a second order one:

Fig. 3: AVISO Global Mean Sea Level (GMSL) derived from satellite altimetry together with the fitted standard trajectory model which includes acceleration.

$$y(t_i) = a + b(t_i - t_0) + c(t_i - t_0)^2 \quad (10)$$

The acceleration is defined as twice the value of c (*Bos et al.*, 2014).

Figure 1 shows a clear linear rise but the acceleration is more difficult to distinguish. We estimate it to be $0.005 \pm 0.002 \text{ mm/yr}^2$, which is thus indeed very small but significant at the two sigma level. An advantage of estimating accelerations is that vertical land motion due to post-glacial rebound, which can for time spans of space geodetic data be considered to be a linear motion, and therefore no longer a source of error. However, tide gauges are historically most common in harbours which over the years get dredged or extended which has an unknown influence on the mean sea-level due to changes in mean ocean currents, see for example (*Araújo et al.*, 2013).

2.2 Absolute sea-level observed with satellite altimetry

Nowadays sea level can also be measured from space using satellite altimetry. the GEOSAT was the first satellite altimetry satellite that provided sea level maps from 1985-1990. Other missions followed such as TOPEX/Poseidon and Jason 1 & 2. In all cases the sea level is given with respect to a frame connected to the centre of the Earth and is therefore absolute. The time series now span over 30 years and the most recent estimate of the acceleration based on satellite altimetry is $0.084 \pm 0.025 \text{ mm/yr}^2$ for 1993-2018, without various geophysical corrections applied (*Nerem et al.*, 2018). These authors used a simple AR(1) noise model to compute the uncertainty of their estimate. They define their ‘noise’ as the difference between the altimetry and tide gauge observations instead of the difference with their fitted model. To study this error estimate, we use the global mean sea-level time series provided by AVISO as shown in Figure 3. This figure clearly shows a secular sea-level rise which appears linear. The acceleration is harder to detect. Also note the large effect of the El Niño Southern Oscillation on sea level in 2012. The power spectral density of the original time series together with the fitted white and AR(1) noise models are shown in Figure 4. At around a period of 30 days, the power drops several orders of magnitude suggesting a low-pass filter has been applied. Therefore, to ensure that this does not influence our results, we averaged sets of 4 consecutive values to form a new time series with a sampling period of approximately 40 days. The corresponding modelled AR(1) noise model is shown as the dotted red line in Figure 4. This

Fig. 4: Power spectral density plot of the AVISO GSML data together with fitted AR(1) and White noise models.

helps to verify that the influence of the high frequency filtering is minimal.

Table 1: Estimated accelerations using various noise models.

The estimated accelerations are listed in Table 1 using a White, AR(1), a GGM and an ARFIMA(1,d,0) noise model. The last three models gave nearly identical results of 0.058 ± 0.020 mm/yr².

These values fall between the result of 0.041 mm/yr² for the period 1993-2014 of *Chen et al.* (2017) and the value of $0.084 + / - 0.025$ mm/yr² for 1993-2018 of *Nerem et al.* (2018). Note that the 0.025 mm/yr² uncertainty of *Nerem et al.* (2018) is the sum of various error sources. What interests us here is their uncertainty of 0.011 mm/yr² associated to the estimation process, using an AR(1) noise model, which is half of our value of 0.020 mm/yr². As explained before, they defined their residuals as the difference between altimetry data and tide gauge data and call it the tide gauge validation error. It might be that these residuals underestimate the real uncertainty of the estimation process or that the AR(1) noise model is too simplistic.

Nevertheless, one must add to this uncertainty various systematic errors such as mismodelling of the orbit and drift of the altimetry amongst others (*Ablain, 2009*). For satellite altimetry data, these systematic errors are larger than the uncertainties associated with the estimation process. One of the strengths of the results of *Nerem et al.* (2018) is their reduction of these systematic errors. This fact might also explain why the simple AR(1) is still widely used in sea-level research. As shown in previous chapters, in GNSS time series the situation is reversed, with estimation errors being larger than the systematic ones and dominating the total uncertainty.

Another aspect which has received little attention is the choice of reference epoch t_0 . If one chooses this to be the middle of the segment, then one allows a good separation of the estimation of the bias, linear trend and acceleration. The separation is perfect in case of no missing data. However, if one chooses another date, the parameters that are to be estimated are correlated, see also *Williams (2014)*. Using our satellite Global Mean Sea Level (GMSL) example, for a t_0 of 1993, the linear trend is 2.6 mm/yr instead of 3.3 mm/yr while the acceleration remains the same.

Next, note that in the literature significant different values of the global mean sea-level accelerations can be found, depending on the length of the

time series that has been analysed. For example, *Yi et al. (2017)* presented an acceleration of $0.27 \pm 0.17 \text{ mm/yr}^2$ for the period 2005-2015 while *Church and White (2011)* obtained an acceleration of $0.013 \pm 0.007 \text{ mm/yr}^2$ for the period 1870-2004. Climate change is a highly non-linear process and a simple constant acceleration might be too simple model due to various decadal variations that are superimposed on the secular motions. A linear sea-level rise describes well the tide gauge observations of the last century, but one should be cautious with the interpretation of quadratic sea-level rise. In contrast to post-glacial rebound and tectonic motion, which are very slow geophysical processes that can be accurately described by linear motions in GNSS time series, secular sea-level variations are much more difficult to capture with a low order polynomial. A good review of the difficulties of fitting a trend to sea-level observations has been published in *Visser et al. (2015)*. For that reason, some researchers dismiss fitting a polynomial and apply other techniques such as wavelet filtering.

2.3 Reference Frame and Vertical Land Motion

So far we have dealt with changes in the sea level. However, as we noted in the Introduction, relative sea-level needs to be converted into absolute sea-level using VLM observations. The first step to measure VLM regionally is to create an internally consistent, hemisphere-scale reference frame. Some studies, such as *Mazzotti et al. (2007)* in the Pacific Northwest, circumvented this problem by defining a small network. *Mazzotti et al. (2007)* defined for their study a local network in the east of Vancouver Island and holding a single inland station (DRAO) fixed. However, large regional or continental scale analyses require a different approach, due to the rates amplitude of ubiquitous and readily measured continental deformation rivalling with coastal VLM rates (*Herring et al., 2016*). In ITRF08, for instance, the reference station DRAO used by *Mazzotti et al. (2007)* has a radial velocity of $0.7 \pm 0.01 \text{ mm/yr}$ based on 27 years of continuous measurements.

In sea-level studies, the estimated VLM relative to Earth's center of mass should ideally be associated with a standard error of approximately an order of magnitude lower than the contemporary climate signals (i.e. 1–3 mm/yr) recorded on average in sea-level time series at tide gauges or in satellite observations (*Wöppelmann and Marcos, 2016*). Moreover, tight constraints on the rate of offset between Earth's center of mass and Earth's center of figure are required, as defined by those GPS stations used to realize the reference frame. In other words, a correlated bias can be produced by any nonzero rate over hemisphere spatial scales in inferred sea-level rise rates. Recent studies, such as *Santamaría-Gómez et al. (2017)*, have addressed this issue to conclude that Earth's center of figure is drifting $0.0 \pm 0.3 \text{ mm/yr}$ along the Earth's rotation axis. A latitude dependent bias can be produced by a nonzero motion between

tide gauge SLR rates and their VLM correction using GPS (within the ITRF reference frame). However, one of the geodesy Grand Challenge (*Davis et al.*, 2012) is our current limitation in the realization of the terrestrial reference frame with a combination of observations from multiple techniques including VLBI, SLR, and GPS (e.g., *Altamimi et al.*, 2011, 2016).

2.4 Estimation of Vertical land Motion

VLM at tide gauges is observed with GPS and is modelled by a linear motion. In addition, the trajectory model should account for offsets introduced by hardware changes or seismic events. All these parameters have a significant influence on the estimated rate (*Gazeaux et al.*, 2013). Transient tectonic processes such as slow slip events also can have an impact on the estimated motions, requiring ideally a proper modeling with a slip inversion for each event. In *Montillet et al.* (2018), the authors postulated a constant contribution of the slow slip events to VLM over long periods, together with a model of the linear process which includes both slow earthquake offsets and long-term interseismic strain.

Here, the functional model used to model daily positions GPS time series includes a linear trend, a seasonal variation with periods fixed to annual and semi-annual and constant phase and amplitude, along with step functions at hardware changes and known seismic events greater than Mw 5.6. (*Bevis and Brown*, 2014) calls this the Standard Linear Trajectory Model which is also discussed in Chapter 1. To separate the annual signal from the linear trend, one requires to record observations for a minimum of approximately 2.5 years at any station (*Blewitt and Lavallée*, 2002).

GPS time series contain correlated noise which can be described by a white plus power-law noise model (*Williams*, 2004). This is slightly different from the case of sea-level time series where only one type of correlated noise was present. The fact that we now need to sum two different noise models, white and power-law, makes it difficult to decompose the covariance matrix directly into two lower triangles \mathbf{L} using the equation of the previous section (*Langbein*, 2017). The traditional approach is therefore to sum the white and power-law noise covariance matrices and afterwards perform a Cholesky decomposition to obtain the lower triangle \mathbf{L} . For the rest the maximum likelihood estimation scheme remains the same.

3 Application to the Estimation of Sea-Level Rise in the Pacific Northwest

3.1 VLM and Tectonic Pattern of the Cascadia region

The first step is to establish a VLM profile for the stations located on the coast in the Pacific Northwest (Vancouver Island to Northern California). The continuous VLM profile is generated by using 100 permanent GPS stations from the Pacific Northwest Geodetic Array (PANGA) (Miller et al., 1998) and EarthScope Plate Boundary Observatory (UNAVCO, 2009), computed within the ITRF 2008 reference frame (e.g., *Altamimi et al.*, 2011). These stations are continuously operating and blanket Cascadia, from northern California through Oregon, Washington State, southwestern British Columbia and Vancouver Island. In order to estimate a smooth VLM profile in the Pacific Northwest, we have selected 47 stations located on or within 10 km of the coast boarding the Pacific ocean, Puget Sound and Salish Sea east of Vancouver Island. Most selected GPS stations have been continuously operating between 10 to over 20 years. Thus, the estimation of the functional model described in the previous section together with the stochastic noise model for these very long time series, allows calculating an accurate long-term vertical land motion rate at an order of magnitude of a few tenths of mm/yr (*Montillet et al.*, 2018).

For GPS data processing, raw GPS phase and code observations were point-positioned with ambiguity resolution using GIPSY/OASIS II, the GPS Inferred Positioning System/Orbit Analysis and Simulation software developed and supported by NASA Jet Propulsion Laboratory (JPL) (*Zumberge*, 1997). Satellite ephemerides, clock corrections, and wide-lane phase bias estimates were provided by JPL (*Bertiger et al.*, 2010).

We choose in our processing that the station positions are loosely constrained during initial estimation and subsequently transformed into the ITRF08 (e.g., *Altamimi et al.*, 2011) using only the translation and rotation, but not scale, components of the JPL-provided Helmert transformations. The use or omission of the scale term in reference frame realization is a matter of debate in the community (see (*Herring et al.*, 2016), (*He et al.*, 2017) and *Montillet et al.* (2018) for a comprehensive discussion). According to *Montillet et al.* (2018), depending on how the scale term is included in the Helmert transformation, subtle differences arise in the reference frame definition that can also have first-order impacts on vertical rate estimates.

The tectonic pattern of the Cascadia region has been intensively studied with GPS measurements in the early 90s' (e.g., *Hyndman and Wang*, 1995; *McCaffrey et al.*, 2007, 2013; *Melbourne et al.*, 2005; *Miller et al.*, 2002). The primary tectonic signal stems from subduction of the Juan de Fuca plate beneath North America at roughly 40 mm/yr (*Wilson*, 1993). Figure 5 shows

Fig. 5: Vertical land motion of the Cascadia subduction zone including British Columbia [A], British Columbia and Washington [B], Oregon [C], Oregon and Northern California [D]. Only coastal stations are used to derive the vertical land motion profiles shown in Figure 6 and 7. Note the change of length of 2 mm/yr scale bar between different boxes. (*Montillet et al.*, 2018)

the vertical land motion varying regionally but smoothly, from the Brooks Peninsula of Vancouver Island at the northern end of the Cascadia margin southward to the southern terminus of the Cascadia margin at Cape Mendocino, California.

Overall, the VLM in the Cascadia fore arc is separated into three regions. All of Vancouver Island and the Olympic peninsula (Cascadia’s northern half) display high uplift rates of almost 5 mm/yr at Woss, BC and Quadra Island, BC, and with a mean uplift of around 2 mm/yr. The large uplift values estimated on Vancouver Island originates from the superposition of subduction interseismic strain and postglacial rebound. These results agree with *Mazzotti et al.* (2007). Furthermore, large uplift rates of approximately 4 mm/yr are observed along the western Olympic Peninsula of northwestern Washington State. The values tend to diminish southward to almost zero south of central coastal Washington and remain near zero to near the latitude of Cape Blanco, Oregon. The mean uplift estimates increase again South of Cape Blanco (about 1–2 mm/yr), reaching a maximum value of 4 mm/yr at Crescent City, California, then dropping again to zero at Cape Mendocino, California. In contrast, the inland waterways of the Puget Sound are characterized by subsidence at rates of 20 mm/yr while the Salish Sea region east of Vancouver Island is marked by uplift ranging from 1 to 4 mm/yr (e.g., Figure 7).

Table 2: GPS-Derived Vertical Land Motion Rate Estimates for Reference Stations Included in PANGA, PBO, and *Mazzotti et al.* (2007) processing. (*Montillet et al.*, 2018)

The PANGA and *Mazzotti et al.* (2007) uplift estimates are listed in Table 2. 67% of the stations processed with the PANGA methodology, show the same rates within 1 sigma, whereas 97% are within 2 sigma. Looking at this table, the mean values estimated using the first eight stations, are 1.34 ± 1.07 mm/yr for PANGA, whereas the mean value is equal to 1.62 ± 1.20 mm/yr using the estimates from *Mazzotti et al.* (2007), which is 23% larger on average. Note that *Mazzotti et al.* (2007) utilized shorter time series (< 7 yrs) modeled with least squares in the *IGS08* reference

Fig. 6: Interpolated long-term steady-state VLM in the Pacific Coast (Washington (WA), Oregon (OR), California (CA), and British Columbia (BC)). Note that the red band is the interpolated uncertainties. The tide gauges are localized by a green star together with their associated number. (*Montillet et al., 2018*)

Fig. 7: Interpolated long-term steady-state VLM in Puget Sound-Salish Sea corridors in Washington State (WA) and British Columbia (BC). The red band is the interpolated uncertainties. Note that station with (*) is in BC and (**) in WA. The confusion is due to the very close latitudes of the stations at the border between BC and Washington State. The tide gauges are localized by a green star together with their associated number. (*Montillet et al., 2018*)

frame, thus impacting the noise properties of the time series compared to *ITRF08*. Therefore the difference in processing methodology should explain the results. Also, looking at the large discrepancy of the uplift estimates at some stations (e.g., PTRF, BLYN), we cannot exclude possible outliers or mismodeling the stochastic processes with our choice of the stochastic noise model for the GPS time series (i.e. Flicker noise with white noise). While the VLM rates are measured along the coast at 47 disparate GPS stations that their inferred rates are smoothly varying allows their interpolation to generate continuous VLM profiles. Note that in Figure 6 and Figure 7, the VLM profile is obtained by linear interpolation of the uplift estimates. This continuous profile can be utilized for SLR adaptation planning by communities where local GPS is not available in order to correct observations recorded by tide gauges.

3.2 Estimation of the Relative Sea-Level Rise

We selected 18 stations along the Pacific Northwest coast in order to estimate the relative sea-level rise (RSLR) rates uncorrected for VLM. These stations are located between the latitudes 40° and 51° . At each tide gauge, monthly records were downloaded from the Permanent Service for Mean Sea Level [PSMSL] (*Holgate et al., 2013*), which in some cases have nearly 115 years of measurements (e.g., Seattle). The RSLR rates are estimated taking into account the presence of coloured and other noise sources as described in the previous sections. Table 3 shows different estimates of the uncorrected RSLR for five tide gauges along coastal Pacific Northwest, Puget Sound, and Salish Sea. As shown in Tables 3 and 4, our RSLR results are generally closer to the values estimated from the NRC group (*NRC, 2015*). The FARIMA model

Table 3: Estimated relative sea-level rise (RSLR) around Pacific Northwest at selected stations. Note for each noise model (ARMA(p,q), ARFIMA(p,d,q), GGM), the optimum lags p and q are selected either by minimizing the AIC or BIC (*Burnham and Anderson, 2002*). Our results are compared with previous studies (*Douglas, 1991; Mazzotti et al., 2007; Wöppelmann et al., 2009; Sweet et al., 2014; NRC, 2015*). μ is the estimated RSLR with σ the associated uncertainty. Uncertainties are one sigma. *Montillet et al. (2018)*

Fig. 8: Red: uncorrected (biased by vertical land motion) Cascadia sea-level rise (SLR) rates estimated from long-term ($\sim 50\text{--}100$ yr) tide gauge measurements; Blue: after correction for interpolated GPS-measured vertical land motion (absolute) at 18 tide gauges around the Pacific Northwest. Note that the full name of the tide gauges are displayed in Table 4. We display a zoom of the main figure (i.e., zoom of box A) due to a visual issue to separate the ones with close latitudes. The black line is the ensemble of GIA models from *NRC (2015)*. Tide gauge trends estimated with GGM noise model. (*Montillet et al., 2018*)

seems to produce smaller uncertainties (using the AIC). Assuming that the AIC selects the lags more optimally than the BIC, it may suggest the presence of long memory processes (i.e., power-law noise) in the TG time series, which should be better accounted for using this stochastic model than using a model such as the ARMA. Even though we have circumvented the bias due to mismodeling the TG measurements using information criteria, we acknowledge that estimated RSL values are sensitive to the choice of record length of the tide gauges selected following previous studies (*Douglas, 1991*) and that unmodeled multidecade transients will impact rate estimates differently based on both the time series duration and the structure of any known long-term transients. Note that the optimality of model selection using information criteria is an active research area within the geophysical community (*He et al., 2017*). RSLR (red) is displayed in Figure 8 as a function of

Table 4: Estimation of the Relative SLR(RSLR) and corrected RSLR with interpolated GPS uplift velocities. (*Montillet et al., 2018*)

latitude, estimated from the tide gauge uncorrected for VLM. RSLR values are scattered along coastal Cascadia, between -2 and $+5$ mm/yr. This result is expected due to the combination of various geophysical processes, in particular the highly variable tectonic and GIA activity together with the intrinsic scatter of average sea-level itself due to the various hydrodynamic

processes controlling yearly regional variations (*Church et al.*, 2004). These RSLR estimates agree with previous studies (e.g., *Mazzotti et al.*, 2007; *Sweet et al.*, 2014; *NRC*, 2015). Thus, their dependence on the choice of the stochastic noise model using the AIC or BIC criteria is relatively minor (at ~ 0.1 sigma confidence level). Uncertainties are computed using the MLE as implemented in the Hector software (*Bos et al.*, 2013b), producing realistic values less sensitive to anomalies (i.e. estimates produced during windy or stormy time periods). Note that at Astoria (Oregon), the RSLR estimate can be assimilated as an outlier, because of the uncertainties larger than the computed linear trend. The station lies 10 km from the coast up the Columbia River estuary. Therefore, we infer that the river itself likely controls much of apparent sea-level fluctuation, consistent with *Mazzotti et al.* (2007) and *Sweet et al.* (2014). Also the tide gauge closed to the GPS station CHZZ has not been used, due to the overall low quality of the raw observations.

3.3 Discussion on the Absolute Sea-Level Rise and Sources of Error

The Absolute sea-level rise (ASLR) is defined as the sum of uncorrected sea-level rise or RSLR, estimated at each tide gauge, with the addition of the VLM measurements inferred from the daily position GPS time series. We use the interpolated value from the VLM coastal profile closest to each of the 18 tide gauges in order to compute the ASLR. The PANGA GPS uplift velocities is chosen because of the large number of stations. In addition, the permanent stations included in both PANGA and PBO processing systems show no significant differences at the one sigma confidence interval. Figure 8 displays the RSLR and the ASLR in the Pacific Northwest. The figure also includes a measure of the Glacial Isostatic Adjustment (GIA) using an ensemble of models. The VLM correction to the RSLR estimates includes both GIA and tectonic strain accumulation. However, it is difficult to accurately isolate the two sources of uplift with imperfect knowledge of mantle viscosity, recent glaciation history, and interseismic coupling along the Cascadia megathrust fault. The GIA models come from *NRC* (2015), and include various contributions such as the changes in geocentric (absolute) sea-level and VLM.

Finally, the figure also shows that the large scattering of the RSLR measurements, is reduced after correction for VLM, to a cluster around 2 mm/yr of ASLR. Prior to correction the mean of the RSLR measurements are 0.526 ± 1.59 mm/yr, whereas after correction they 1.996 ± 1.18 mm/yr. These values are consistent with other studies of the SLR measurements in the northeastern Pacific (e.g., *Church et al.*, 2004; *Wöppelmann et al.*, 2009; *NRC*, 2015). Regionally based on the ARMA estimates, along the outer Pacific coast of

Washington State the ASLR rate is 1.366 ± 0.76 and 2.406 ± 1.41 mm/yr on Vancouver Island. These values are in the high end of the interval defined by the estimates from previous studies of the twentieth century global mean sea-level rise (*Church and White, 2011*). Along coastal Oregon ASLR averages 1.666 ± 0.97 mm/yr, and for northern California 1.996 ± 1.14 mm/yr. This drop in uncertainty may suggest that the VLM correction absorbs much of the regional scatter in tide gauge SLR estimates. Also the study profiles expected rebound associated with GIA, drawn from an ensemble of models computed in *NRC (2015)*, which suggest that roughly half the VLM on Vancouver Island arise from GIA and the rest from subduction-related strain accumulation.

4 Conclusions on Global Mean Sea-Level

In this chapter we have shown that also tide gauge and satellite altimetry time series contain correlated noise. Since this noise can be described by a single noise model, not a sum of various models, we presented the recent efficient maximum likelihood method of *Langbein (2017)* to estimate the noise parameters and the sea-level rate. Furthermore, we emphasised that in contrast to linear sea-level rise, sea-level acceleration is much harder to detect. In addition, the estimated acceleration seems to depend on the time span used which might indicate that a simple acceleration is not an adequate model for the highly nonlinear processes that take place within the ocean.

Tide gauges only observe relative sea level and GPS derived vertical motion is needed to convert these values into absolute sea level rise. To illustrate this process, we presented tide gauge and GPS time series from the Northwest Pacific. In this region the rates are more similar to twenty first century global rates (3.16 ± 0.7 mm/yr), whereas eastern Pacific satellite rates are significantly lower than the global mean value. Much of the west coast of the Americas actually show an apparent decrease in satellite geocentric sea surface height over the last 20 years (*Church and White, 2011*). For tide gauge measurements, many studies have also underlined how they are impacted by many processes that can vary from hemispherical, most notably the Pacific decadal oscillation, to spatially localized, and which may act over timescales over roughly a year to several decades. Such processes alter surface winds, ocean currents, temperature, and salinity, and, in turn sea-level, all superimposed on long-term background sea-level rise (e.g., *Church et al., 2004; Nicholls and Cazenave, 2010; Church and White, 2011; Cazenave and Le Cozannet, 2013; IPCC, 2013; Cazenave et al., 2014; Hay et al., 2015*). Therefore tide gauges-based mean sea-level exhibits large interannual variability compared with the global mean value estimated from satellite altimetry. However, the values are the same order of magnitude to regional measurements reported by satellite altimetry (*Prandi et al., 2009*). In the

Pacific Northwest, ASLR mean reported here of 1.36 ± 0.75 mm/yr is $\sim 20\%$ smaller than the 1.7 mm/yr global mean SLR from 1901 to 2010 (*IPCC*, 2013). However, if we take into account Vancouver Island, the ASLR is around 1.99 ± 1.18 mm/yr and thus $\sim 17\%$ higher than the global mean SLR.

Finally, coastal communities facing the risk of rapid sea-level rise should utilize sea-level projections and flooding maps to develop with local authorities a strategy for long-term adaptation imposed by the effects of climate change. In the Pacific Northwest, the average absolute SLR obtained after accounting for VLM yields, for coastal Cascadia, roughly 2 mm/yr, very similar to the 2 mm/yr previously described with other global observations (e.g., *Church et al.*, 2004; *NRC*, 2015). Within Puget Sound widespread subsidence identified with GPS shows that rate of SLR will be exacerbated.

Thus, the methodology developed in *Montillet et al.* (2018) by estimating a smooth VLM profile along the coast with the large number of permanent GPS stations available in the Cascadia region, and then interpolating the value to correct the RSLR at each tide gauge, can be replicated around the world, knowing the sheer numbers of GPS stations now available (over 16,000 globally (*Blewitt et al.*, 2016)) and leaving just a few coastlines unmeasured.

Acknowledgements Timothy Melbourne, Jean-Philippe Montillet and Walter Szeliga would like to acknowledge that their work was supported by the National Aeronautics and Space Administration Research Opportunities in Solid Earth Science Grant No. *NNX10AD15G*. Operations of the Pacific Northwest Geodetic Array, including archiving and daily analysis of GNSS data, was supported by the USGS National earthquake Hazards Reduction Program Cooperative Agreement *G15AC00062*. Raw GPS observations from PANGA GPS stations can be downloaded at the website (<http://www.panga.cwu.edu/data/bysite/>) for the PANGA stations and UNAVCO (<ftp://data-out.unavco.org/pub/products/position/>) for the PBO(-NMT) stations. Data from the EarthScope Plate Boundary Observatory were used in this study. Tide gauge time series are downloaded from the Permanent Service for Mean Sea Level (PSMSL) website.

The work carried out by Machiel Bos and Rui Fernandes was sponsored by national Portuguese funds through FCT in the scope of the project IDL-FCT- UID/GEO/50019/2019 and grant number SFRH/BPD/89923/2012. Computational resources were provided by C4G – Collaboratory for Geosciences (PINFRA/22151/2016).

References

- Ablain M., Cazenave A., Valladeau G., Guinehut S. (2009), A new assessment of the error budget of global mean sea level rate estimated by satellite altimetry over 1993-2008, *Ocean Sci.*, 5, 193–201, doi:10.5194/os-5-193-2009.
- Agnew D.C. (1992), The time-domain behaviour of power-law noises, *Geophys. Res. Lett.*, 19(4), 333–336, doi:10.1029/91GL02832.

- Akaike H. (1974), A new look at the statistical model identification, *Auto. Cont., IEEE Trans. on*, 19(6), 716-723, doi:10.1109/TAC.1974.1100705.
- Altamimi Z., Collilieux X., Métivier L. (2011), ITRF2008: an improved solution of the international terrestrial reference frame, *J. of Geod.*, 85, vol. 8, 457-473, doi:10.1007/s00190-011-0444-4.
- Altamimi Z., Rebischung P., Métivier L., Collilieux X. (2016), ITRF2014: A new release of the International Terrestrial Reference Frame modeling nonlinear station motions, *J. Geophys. Res. Solid Earth*, 121, 6109-6131, doi:10.1002/2016JB013098.
- Araújo I. B., Bos M.S., Bastos L.C., Cardoso M.M. (2013), Analysing the 100 year sea level record of Leixões, Portugal , *J. of Hydro.*, 481, 76-84, doi: 10.1016/j.jhydrol.2012.12.019.
- Beran J. (1992), Statistical methods for data with long-range dependence, *Stat. Sci.*, 7(4), 404-416, doi:10.1214/ss/1177011127
- Bertiger W., Desai S.D., Haines B., Harvey N., Moore A. W., Owen S. , Weiss J.P. (2010), Single receiver phase ambiguity resolution with GPS data, *J. Geod.*, 84, 327-337, doi:10.1007/s00190-010-0371-9.
- Bevis M., Brown A. (2014), Trajectory models and reference frames for crustal motion geodesy, *J. Geod.*, 88(3), 283-311, doi:10.1007/s00190-013-0685-5.
- Blewitt G., Lavallée D. (2002), Effect of annual signals on geodetic velocity, *J. of Geophys. Res.*, 107, B2145, doi:10.1029/2001JB000570.
- Blewitt G., Kreemer C., Hammond W.C., Gazeaux J. (2016), MIDAS Robust Trend Estimator for Accurate GPS Station Velocities Without Step Detection, *J. Geophys. Res. Solid Earth*, 121, doi:10.1002/2015JB012552.
- Bos M. S., Fernandes R.M.S., Williams S.D.P., Bastos L. (2008), Fast error analysis of continuous GPS observations, *J. Geod.*, 82 (3), 157-166, doi:10.1007/s00190-007-0165-x.
- Bos M.S., Fernandes R.M.S., Williams S.D.P., Bastos L. (2013), Fast Error Analysis of Continuous GNSS Observations with Missing Data, *J. Geod.*, 87(4), 351-360, doi:10.1007/s00190-012-0605-0.
- Bos M.S., Araújo I. B., Bastos L. (2013b), Hector user manual version 1.1.
- Bos, M.S., Williams S. D. P., Araújo I. B., Bastos L. (2014), The effect of temporal correlated noise on the sea level rate and acceleration uncertainty, *Geophys. J. Int.*, 196(3), doi: 10.1093/gji/ggt481.
- Burnham K.P., Anderson D. R. (2002), Model selection and mulitmode inference: a practical information-theoretic approach, Springer-Verlag, New-York, Inc., 2nd Edition.
- Cazenave A., Le Cozannet G. (2013), Sea level rise and its coastal impacts, *Earth's Future*, 2, 15-34, doi:10.1002/2013EF000188.
- Cazenave A., Dieng H. B., Meyssignac B., von Schuckmann K., Decharme B., Berthier E. (2014), The rate of sea-level rise, *Nat. Clim. Change*, 4, 358-361, doi:10.1038/nclimate2159.
- Chandler, R. E., Scott E. M. (2011), Statistical Methods for Trend Detection and Analysis in the Environmental Sciences, 368 p., John Wiley, Chichester, U. K.

- Chen X., Zhang X., Church J.A., Watson C.S., King M.A., Monselesan D., Legresy B., Harig C. (2017), the increasing rate of global mean sea-level rise during 1993–2014, *Nat. Clim. Change*, 7(7), p.492, doi:10.1038/nclimate3325.
- Church J., White N.J., Coleman R., Lambeck K., Mitrovica J.X. (2004), Estimates of the regional distribution of sea level rise over the 1950 to 2000 period, *J. Climate*, 17 (13), 2609-2625, doi:10.1175/1520-0442(2004)0172609:EOTRDO2.0.CO.2.
- Church J. A., White N.J. (2006), A 20th century acceleration in global sea-level rise, *Geophys. Res. Lett.*, 33, L01602, doi:10.1029/2005GL024826.
- Church J., Woodworth P. L., Aarup T., Stanley Wilson W. (2010), *Understanding Sea Level and Variability*, Wiley-Blackwell, ISBN: 978-1-444-33452-4.
- Church J. A., White N. J. (2011), Sea-level rise from the late 19th century to the early 21st century, *Surv. Geophys.*, 32 (4-5), 585-602, doi: 10.1007/s10712-011-9119-1.
- Christiansen B., Schmith T., Thejll P. (2010), A surrogate ensemble study of sea level reconstructions, *J. Climate*, 23, 4306–4326, doi: 10.1175/2010JCLI3014.1.
- Colosi, J.A., W. Munk (2006) Tales of the Venerable Honolulu Tide Gauge. *J. Phys. Oceanogr.*, 36, 967–996, doi:10.1175/JPO2876.1
- Dangendorf S., Rybski D., Mudersbach C., Muller A., Kaufmann E., Zorita E., Jensen J. (2014), Evidence for long-term memory in sea-level, *Geophys. Res. Lett.*, 41, 5530-5537, doi:10.1002/2014GL060538.
- Davis J. L., Fialko Y., Holt W. E., Miller M. M., Owen S. E., Pritchard M. E. (Eds.) (2012), *A Foundation for Innovation: Grand Challenges in Geodesy*, Report from the Long-Range Science Goals for Geodesy Community Workshop, UNAVCO, Boulder, Colorado, 79 pp., available at https://www.unavco.org/community/publications_and_reports/geodesy_science_plan/GrandChallengesInGeodesy-Final-Singles-LR.pdf.
- Douglas B. C. (1991), Global sea level rise, *J. Geophys. Res.*, 96(C4), 6981-6992, doi:10.1029/91JC00064.
- Dragert H., Wang K., James T.S. (2001), A Silent Slip Event on the Deeper Cascadia Subduction Interface, *Science*, 292, 1525-1528, doi: 10.1126/science.1060152.
- Gazeaux J., Williams S.D.P., King M., Bos M.S., Dach R., Deo M., Moore A. W. et al. (2013), Detecting offsets in GPS time series: First results from the detection of offsets in GPS experiment, *J. Geophys. Res.*, 118 (5), 2397-2407, doi:10.1002/jgrb.50152.
- Haigh I. D., Wahl T., Rohling E. J., Price R. M., Pattiaratchi C. B., Calafat F. M., Dangendorf S. (2014), Timescales for detecting a significant acceleration in sea level rise, *Nat. Commun.*, 5, 3635, doi:10.1038/ncomms4635.
- Hamlington B. D., Thompson P., Hammond W. C., Blewitt G., Ray R. D. (2016), Assessing the impact of vertical land motion on twentieth century

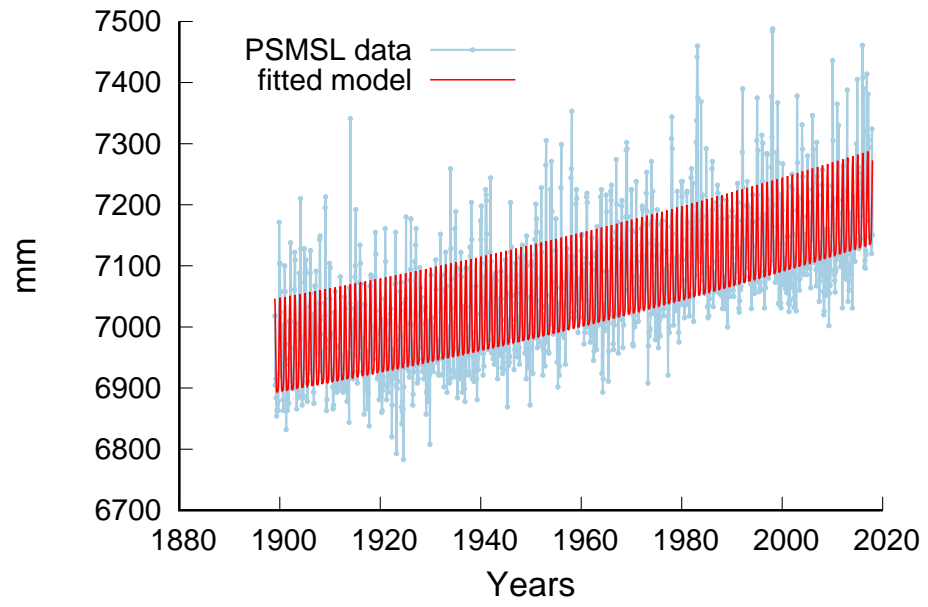
- global mean sea level estimates, *J. Geophys. Res. Oceans*, *121*, 4980-4993, doi:10.1002/2016JC011747.
- Hay C.C., Morrow E., Kopp R.E., Mitrovica J.X. (2013), Estimating the sources of global sea level rise with data assimilation techniques, *Proc. Natl. Acad. Sci.*, *110(Suppl. 1)*, 3692-3699, doi:10.1073/pnas.1117683109.
- Hay C. C., Marrow E., Kopp R. E., Mitrivica J. X. (2015), Probabilistic reanalysis of twentieth-century sea-level rise, *Nature*, *517*, 481-484, doi:10.1038/nature14093
- He X., Montillet J.-P., Hua X., Yu K., Jiang W., Zhou F. (2016), Noise analysis for environmental loading effect on GPS time series, *Acta Geodyn. Geomater.*, *14* (185), 131-142, doi:10.13168/AGG.2016.0034.
- He X., Montillet J.-P., Fernandes R., Bos M., Yu K., Jiang W. (2017), Review of current GPS methodologies for producing accurate time series and their error sources, *J. of Geodyn.*, *106*, 12-29, doi: 10.1016/j.jog.2017.01.004.
- Herring T. A., King R. W., McClusky S. C. (2010), Introduction to GAMIT/GLOBK, *report, Mass. Inst. of Technol.*, Cambridge.
- Herring T. A., King R. W., McClusky S. C., Floyd M., Wang L., Murray M., Melbourne T., Santillan M., Szeliga W., Phillips D., Puskas C. (2016) Plate Boundary Observatory and Related Networks: GPS Data Analysis Methods and Geodetic Products, *Rev. Geophys.*, *54*, 759-808, doi:10.1002/2016RG000529.
- Holgate S. J., Matthews A., Woodworth P.L., Rickards L.J., Tamisiea M.E., Bradshaw E., Foden P.R., Gordon K. M., Jevrejeva S. , Pugh J. (2013), New Data Systems and Products at the Permanent Service for Mean Sea Level, *J. of Coastal Res.*, *29* (3), 493 – 504, doi:10.2112/JCOASTRES-D-12-00175.1.
- Hughes C.W., Williams S.D.P. (2010), The color of sea level: importance of spatial variations in spectral shape for assessing the significance of trends, *J. Geophys. Res.*, *115(C14)*, 10048, doi:10.1029/2010JC006102.
- Hyndman R. D., Wang K. (1995), The rupture zone of Cascadia great earthquakes from current deformation and the thermal regime, *J. Geophys. Res.*, *100(B11)*, 22133-22154, doi:10.1029/95JB01970.
- IPCC (2013), Climate Change 2013: The Physical Science Basis. Contribution of Working Group I to the Fifth Assessment Report of the Intergovernmental Panel on Climate Change, edited by T. F. Stocker et al., Cambridge Univ. Press, Cambridge, U. K.
- Jevrejeva S., Moore J. C., Grinsted A., Woodworth P. L. (2008), Recent global sea level acceleration started over 200 years ago?, *Geophys. Res. Lett.*, *35*, L08715, doi:10.1029/2008GL033611.
- Klos A., Bogusz J., Figurski M., Gruszczynski M. (2015), Error analysis for European IGS stations, *Stud. Geophys. Geod.*, *60*(1) 1-18, doi:10.1007/s11200-015-0828-7.
- Lambeck K., Johnston P. (1995), Land subsidence and sea-level change: Contributions from the melting of the last great ice sheets and the isostatic adjustment of the Earth. In: Land Subsidence-Proceedings of the 5th Inter-

- national Symposium on Land Subsidence, (F.B.J. Barends, F.J.J. Brouwer and F.H. Schroder, Eds), The Hague, Netherlands, Balkema, Rotterdam, 3-18.
- Langbein J. (2004), Noise in two-color electronic distance meter measurements revisited, *J. Geophys. Res.*, *109*(B4), doi:10.1029/2003JB002819.
- Langbein J. (2008), Noise in GPS displacement measurements from Southern California and Southern Nevada, *J. Geophys. Res.*, *113*(B5), doi:10.1029/2007JB005247.
- Langbein, J. (2017) *J Geod*, *91*, 985-994, doi:10.1007/s00190-017-1002-5
- Lyu K., Zhang X., Church J. A., Slangen A. B. A., Hu J. (2014), Time of emergence for regional sea-level change, *Nat. Clim. Change*, *4*, 1006-1010, doi:10.1038/nclimate2397.
- Mao A., Harrison C. G. , Dixon T. H. (1999), Noise in GPS coordinate time series, *J. Geophys. Res.*, *104*(B2), 2797-2816, doi:10.1029/1998JB900033.
- Mazzotti S., Lambert A., Courtier N., Nikolaishen L., Dragert H. (2007), Crustal uplift and sea level rise in northern Cascadia from GPS, absolute gravity, and tide gauge data, *Geophys. Res. Lett.*, *34*, L15306, doi:10.1029/2007GL030283.
- McCaffrey R., Qamar A. I., King R. W., Wells R., Khazaradze G., Williams C. A., Stevens C. W., Vollick J. J., Zwick P. C. (2007) Fault locking, block rotation and crustal deformation in the Pacific Northwest, *Geophys. J. Int.*, *169*, 1315-1340, doi:10.1111/j.365-246X.2007.03371.x.
- McCaffrey, R., King R. W., Payne S. J., Lancaster M. (2013), Active tectonics of northwestern US inferred from GPS-derived surface velocities, *J. Geophys. Res.*, *118*(2), 709-723, doi:10.1029/2012JB009473.
- Melbourne T.I., Szeliga W.M., Miller M., Santillan V.M. (2005), Extent and duration of the 2003 Cascadia slow earthquake, *Geophys. Res. Lett.*, *32*, L04301, doi:10.1029/2004GL021790.
- Meertens C., Boler F. M., Wier S., Blewitt G., Hammond W. C., Kreemer C. (2015), Plug and Play GPS for Earth Scientists: Providing Immediate Access to Low-Latency Geodetic Products for Rapid Modeling and Analysis of Natural Hazards, American Geophysical Union, Fall Meeting 2015, abstract G11B-0983, <http://adsabs.harvard.edu/abs/2015AGUFM.G11B0983M>.
- Miller M. M., Dragert H., Endo E., Freymueller J. T., Goldfinger C., Kelsey H. M., Humphreys E. D., Johnson D. J., McCaffrey R., Oldow J. S., Qamar A., Rubin C. M. (1998), PANGA: Precise Measurements Help Gauge Pacific Northwest's Earthquake Potential, *Eos Transactions, American Geophysical Union*, *79* (23), 269-275.
- Miller M.M., Melbourne T.I., Johnson D.J., Summer W.Q. (2002), Periodic slow earthquakes from the Cascadia subduction zone, *Science*, *295*(5564), doi:10.1126/science.1071193.
- Mitrovica J.X., Davis J.L. (1995), Present-day post-glacial sea level change far from the late Pleistocene ice sheets: Implications for recent analy-

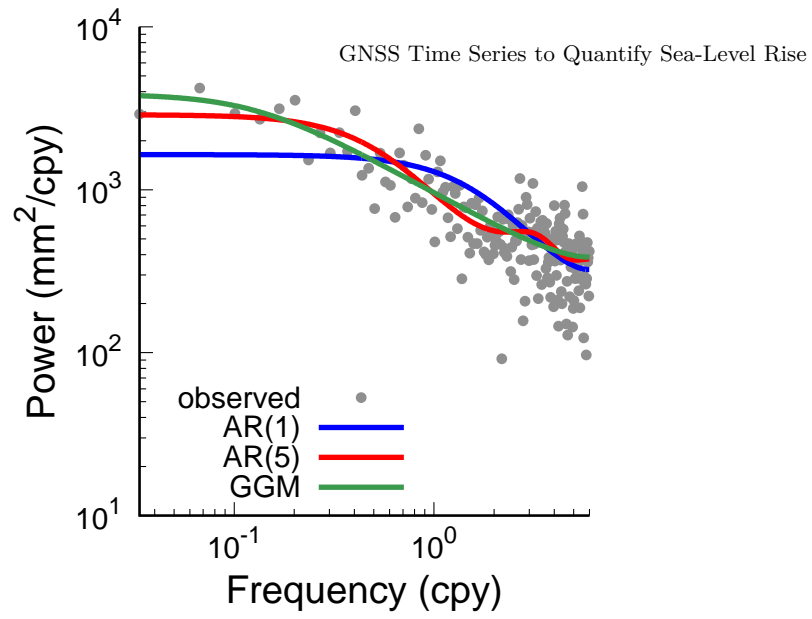
- ses of tide gauge records, *Geophys. Res. Lett.*, *22*(18), 2529-2532, doi: 10.1029/95GL02240.
- Montillet J.P., Williams S. D. P., Koulali A., McClusky S. C. (2015), Estimation of offsets in GPS time-series and application to the detection of earthquake deformation in the far-field, *Geophys. J. Int.*, *200*(2), 1205-1219, doi: 10.1093/gji/ggu473.
- Montillet J.P., Yu K. (2015), Modelling Geodetic Processes with Levy alpha-stable distribution, *Math. Geo.*, *47*(6), 627-646, doi:10.1007/s11004-014-9574-6.
- Montillet J.-P., Melbourne T.I., Szeliga W. M. (2018), GPS vertical land motion corrections to sea-level rise estimates in the Pacific Northwest, *J. of Geophys. Res.*, *123*, doi:10.1002/2017JC013257.
- Nerem R.S., Beckley B.D., Fasullo J.T., Hamlington B.D., Masters D., Mitchum G. T. (2018), Climate-change-driven accelerated sea-level rise detected in the altimeter era, *Proc. Nat. Acad. Sci.*, *115*(9), 2022-2025, doi: 10.1073/pnas.1717312115.
- National Research Council Report (NRC) (2015), Sea-Level Rise for the Coasts of California, Oregon, and Washington: Past, Present, and Future. ISBN 978-0-25594-3. Available at: www.nap.edu/catalog.php?record_id=13389.
- Nicholls R. J., Cazenave A. (2010), Sea-level rise and its impact on coastal zones, *Science*, *328*(5985), 1517-1520, doi:10.1126/science.1185782.
- Panas E. (2001), Estimating fractal dimension using stable distributions and exploring long memory through ARFIMA models in Athens Stock Exchange, *Appl. Fin. Econ.*, *11*(4), 395-402, doi:10.1080/096031001300313956.
- Prandi P., Cazenave A., Becker M. (2009), Is coastal mean sea level rising faster than the global mean? A comparison between tide gauges and satellite altimetry over 1993-2007, *Geophys. Res. Lett.*, *36*(5), L05602, doi:10.1029/2008GL036564
- Press W.H. (1978), Flicker noises in astronomy and elsewhere, *Comment. Astrophys.*, *7*, 103-119.
- Santamaría-Gómez A., Gravelle M., Dangendorf S., Marcos M., Spada G., Wöppelmann G. (2017), Uncertainty of the 20th century sea-level rise due to vertical land motion errors, *Earth Planet Sci. Lett.*, *473*, 24-32, doi.org/10.1016/j.epsl.2017.05.038.
- Schwarz G. (1978), Estimating the dimension of a model, *Ann. of stat.*, *6*(2), 461-464.
- Smith R. A. (2002), Historical golden gate tidal series, *NOAA Tech. Rep.*, NOS CO-OPS 035.
- Sweet W., Park J., Marra J., Zervas C., Gill S. (2014), Sea Level Rise and Nuisance Flood Frequency Change around the Unites States, National Oceanic and Atmospheric Administration (NOAA) Technical Report NOS CO-OPS 073 available at: http://tidesandcurrents.noaa.gov/publications/NOAA_Technical_Report_NOS_COOPS_073.pdf

- Szeliga W., Melbourne T., Santillan V., Miller M. (2008), GPS constraints on 34 slow slip events in the Cascadia subduction zone, 1997-2005, *J. Geophys. Res.*, *113*, B04404, doi:10.1029/2007JB004948.
- Talke, S. A., Kemp, A. C., Woodruff, J. (2018), Relative sea level, tides, and extreme water levels in Boston harbor from 1825 to 2018. *Journal of Geophysical Research: Oceans*, *123*, 3895-3914. doi:10.1029/2017JC013645
- UNAVCO (2009), Plate Boundary Observatory: The first five years. Available at: <https://www.unavco.org/education/outreach/pamphlets/2009-PBO/PBO-2009-brochure-first-five-years.pdf>
- Visser H., Dangendorf S., Petersen A. C. (2015), A review of trend models applied to sea level data with reference to the "acceleration-deceleration debate", *J. Geophys. Res. Oceans*, *120*, 3873-3895, doi:10.1002/2015JC010716.
- Wenzel M., Schroter J. (2014), Global and regional sea level change during the 20th century, *J. Geophys. Res. Oceans*, *119*, 7493-7508, doi:10.1002/2014JC009900.
- Williams S.D.P. (2003), The effect of coloured noise on the uncertainties of rates estimated from geodetic time series, *J. of Geod.*, *76*, doi:10.1007/s00190-002-0283-4.
- Williams S.D.P. (2003b), Offsets in Global Positioning System time series, *J. Geophys. Res.*, *108*, doi:10.1029/2002JB002156.
- Williams S. D., Bock Y., Fang P., Jamason P., Nikolaidis R. M., Prawirodirdjo L., Johnson D. J. (2004), Error analysis of continuous GPS position time series, *J. Geophys. Res.*, *109*(B3), doi:10.1029/2003JB002741.
- Williams, S.D. (2008), CATS: GPS coordinate time series analysis software, *GPS Solut.*, *12*(2), 147-153, doi:10.1007/s10291-007-0086-4.
- Williams S.D.P, Moore P., King M.A., Whitehouse P.L. (2014), Revisiting GRACE Antarctic ice mass trends and accelerations considering autocorrelation, *Earth Planetary Sci. Lett.*, *385*, 12-21, doi:10.1016/j.epsl.2013.10.016.
- Wilson D.S. (1993), Confidence intervals for motion and deformation of the Juan de Fuca plate, *J. Geophys. Res.*, *98*, B9, 16053-16071, doi:10.1029/93JB01227.
- Wöppelmann G., Martin Miguez B., Bouin M.-N., Altamimi Z. (2007), Geocentric sea-level trend estimates from GPS analyses at relevant tide gauges world-wide, *Global Planet. Change*, *57*, 396-406, doi:10.1016/j.gloplacha.2007.02.002.
- Wöppelmann G., Letetrel C., Santamaria A., Bouin M.-N., Collilieux X., Altamimi Z., Williams S. D. P., Martin Miguez B. (2009), Rates of sea-level change over the past century in a geocentric reference frame, *Geophys. Res. Lett.*, *36*, L12607, doi:10.1029/2009GL038720.
- Wöppelmann, G., Marcos M. (2016), Vertical land motion as a key to understanding sea level change and variability, *Rev. Geophys.*, *54*, 64-92, doi:10.1002/2015RG000502.

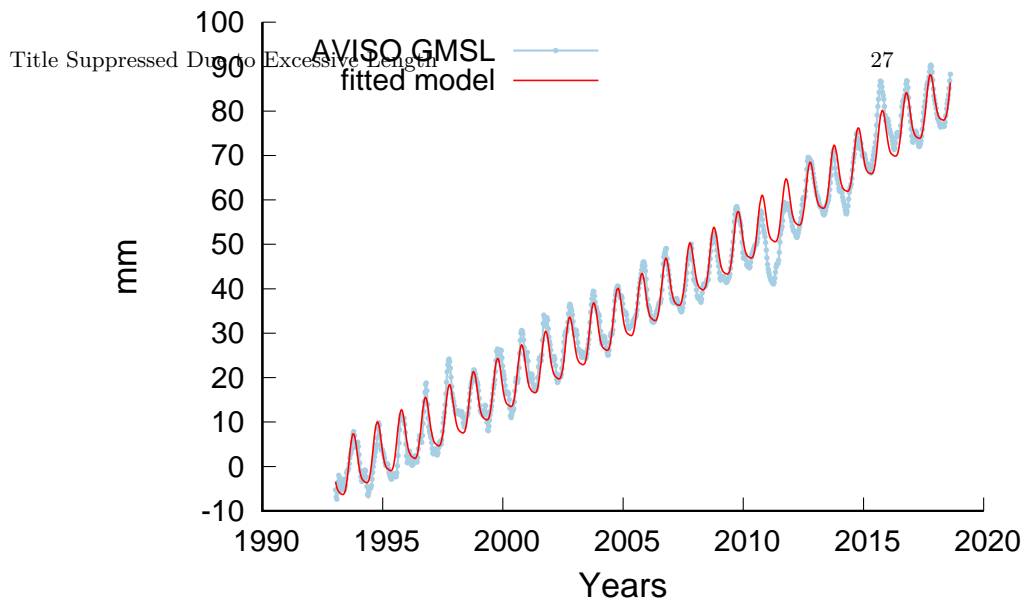
- Yi S., Heki K., Qian A. (2017), Acceleration in the global mean sea level rise: 2005–2015, *Geophys. Res. Lett.*, *44* (11), 905–11,913, doi:10.1002/2017GL076129.
- Zhang J., Bock Y., Johnson H., Fang P., Williams S., Genrich J., Behr J. (1997), Southern California Permanent GPS Geodetic Array: Error analysis of daily position estimates and site velocities, *J. Geophys. Res.*, *102*(B8), 18035-18055, doi:10.1029/97JB01380.
- Zumberge J.F., Heflin M.B., Jefferson D.C., Watkins M.M., Webb F. H. (1997), Precise point positioning for the efficient and robust analysis of GPS data from large networks, *J. Geophys. Res.*, *102*, doi: 10.1029/96JB03860.



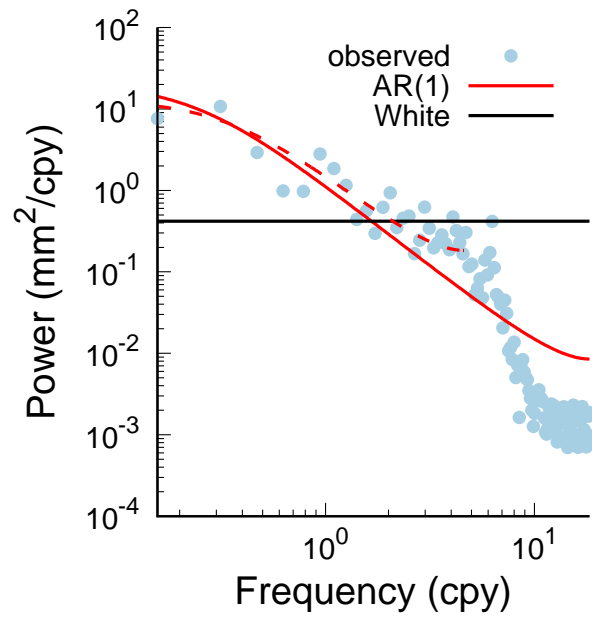
Monthly tide gauge data from Seattle (source PSMSL) with the fitted trajectory model.



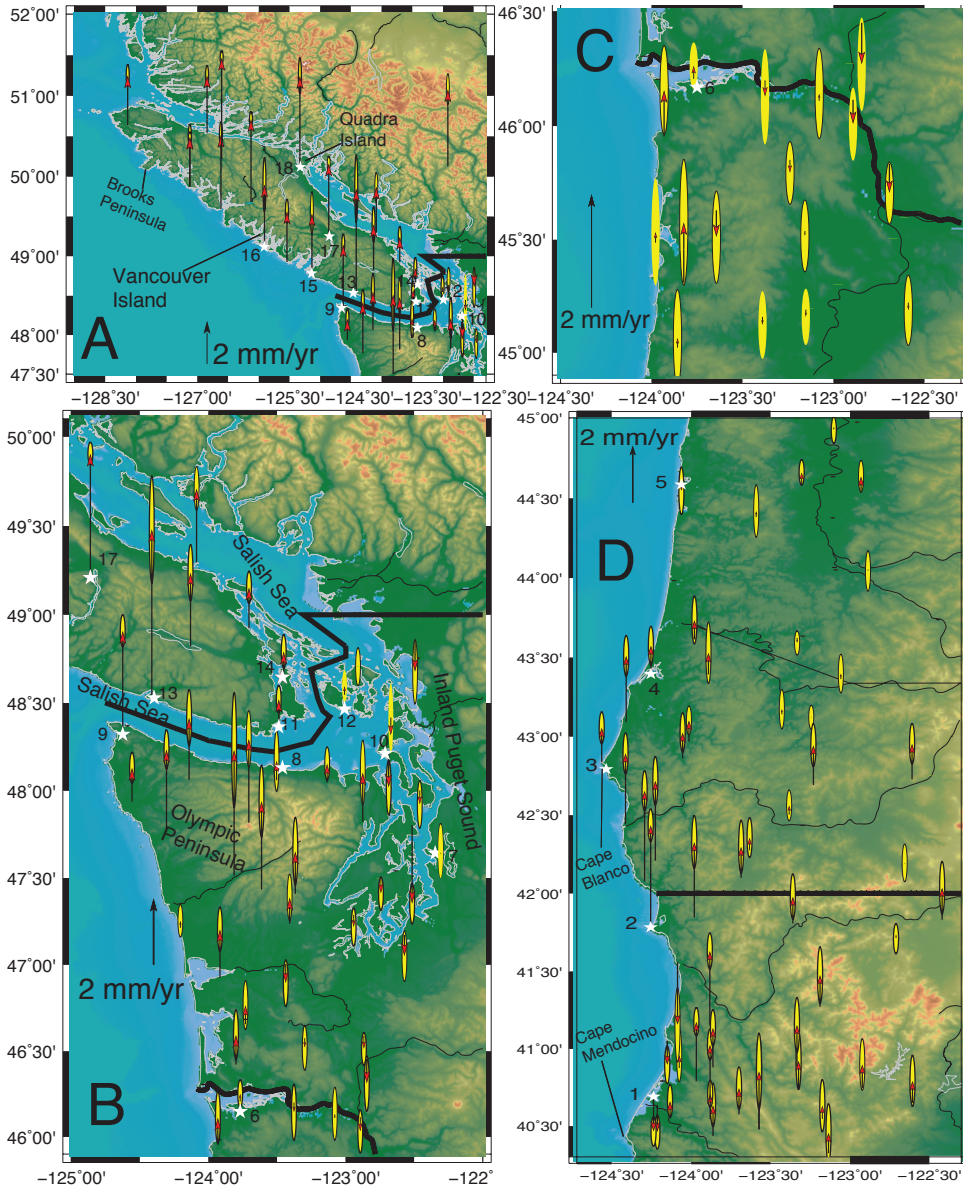
Power spectral density plot of the residuals for the Seattle monthly tide gauge data. Fitted are the power spectra using an AR(1), AR(5) and GGM noise model.



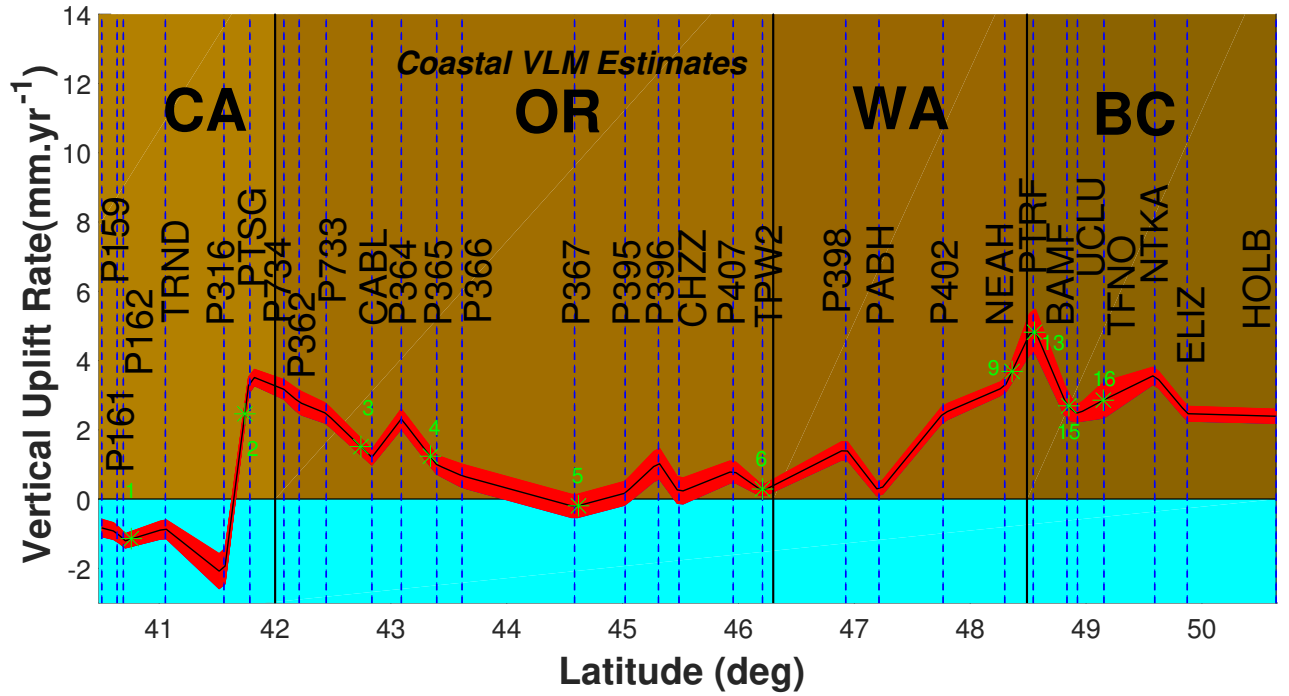
AVISO Global Mean Sea Level (GMSL) derived from satellite altimetry together with the fitted standard trajectory model which includes acceleration.



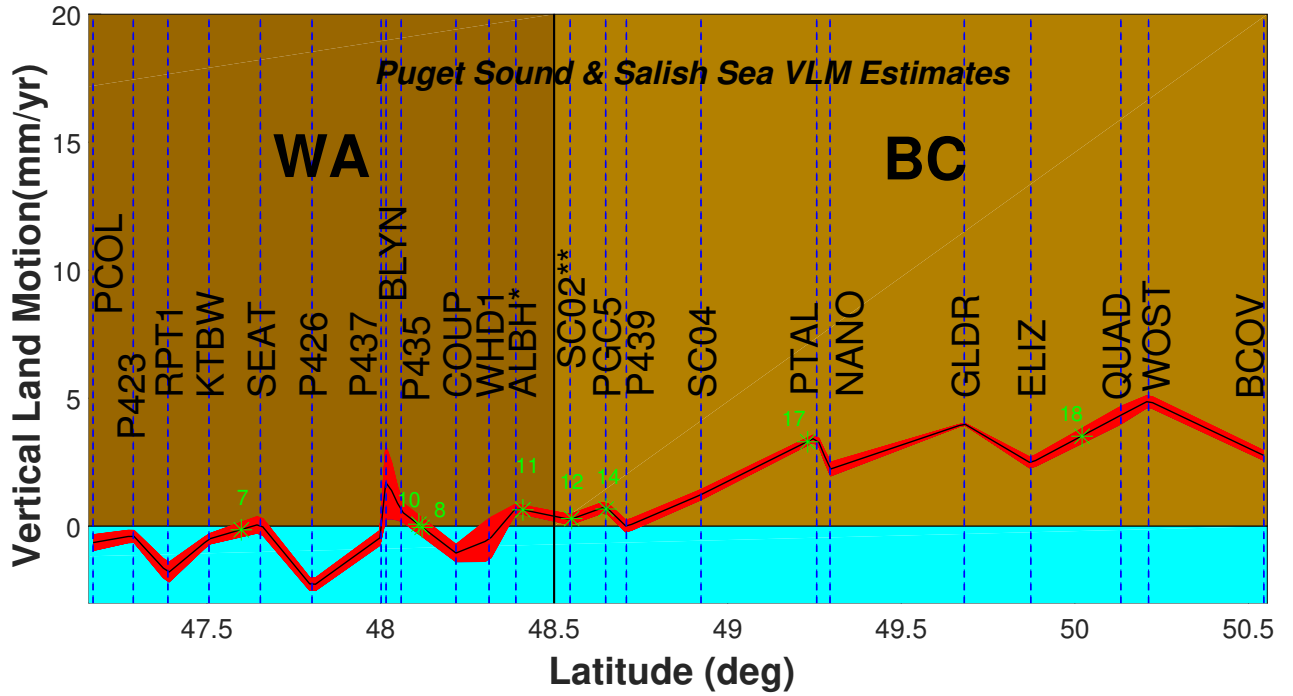
Power spectral density plot of the AVISO GSML data together with fitted AR(1) and White noise models.



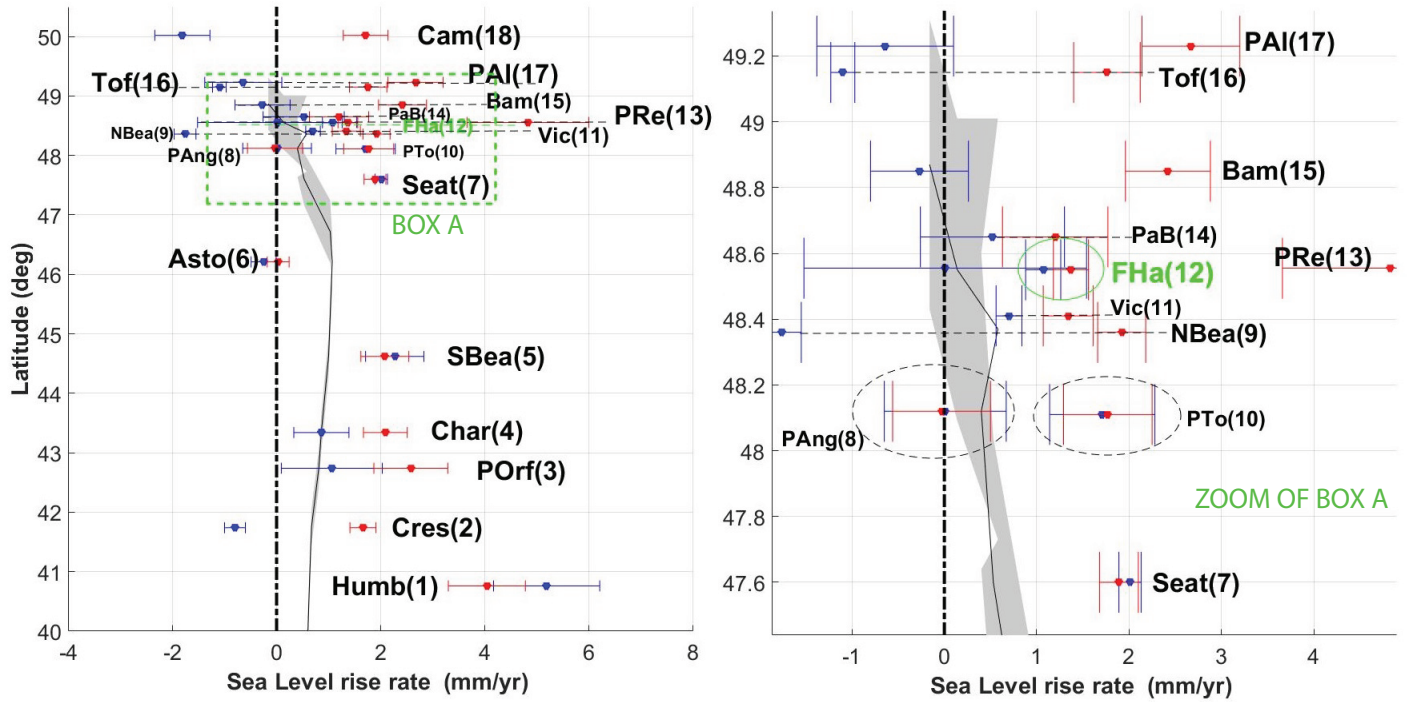
Vertical land motion of the Cascadia subduction zone including British Columbia [A], British Columbia and Washington [B], Oregon [C], Oregon and Northern California [D]. Only coastal stations are used to derive the vertical land motion profiles shown in Figure 6 and 7. Note the change of length of 2 mm/yr scale bar between different boxes. (Montillet *et al.*, 2018)



Interpolated long-term steady-state VLM in the Pacific Coast (Washington (WA), Oregon (OR), California (CA), and British Columbia (BC)). Note that the red band is the interpolated uncertainties. The tide gauges are localized by a green star together with their associated number. (*Montillet et al.*, 2018)



Interpolated long-term steady-state VLM in Puget Sound-Salish Sea corridors in Washington State (WA) and British Columbia (BC). The red band is the interpolated uncertainties. Note that station with (*) is in BC and (**) in WA. The confusion is due to the very close latitudes of the stations at the border between BC and Washington State. The tide gauges are localized by a green star together with their associated number. (Montillet *et al.*, 2018)



Red: uncorrected (biased by vertical land motion) Cascadia sea-level rise (SLR) rates estimated from long-term ($\sim 50 - 100$ yr) tide gauge measurements; Blue: after correction for interpolated GPS-measured vertical land motion (absolute) at 18 tide gauges around the Pacific Northwest. Note that the full name of the tide gauges are displayed in Table 4. We display a zoom of the main figure (i.e., zoom of box A) due to a visual issue to separate the ones with close latitudes. The black line is the ensemble of GIA models from NRC (2015). Tide gauge trends estimated with GGM noise model. (Montillet *et al.*, 2018)

Estimated accelerations using various noise models.

Noise model	Acceleration mm/yr^2
White Noise	0.060 \pm 0.008
AR(1)/ARFIMA(1,d,0)/GGM	0.058 \pm 0.020

GPS-derived vertical land motion rate estimates for reference stations included in PANGA, PBO and *Mazzotti et al.* (2007) processing. μ is the estimated velocity, σ is the associated uncertainty. Uncertainties are one sigma. PANGA and PBO-NMT results are computed using Hector. NaN means that the station was not available. *Montillet et al.* (2018)

			PANGA		NMT		<i>Mazzotti et al.</i> (2007)	
	Lat.	Lon	μ	σ	μ	σ	μ	σ
ALBH	48.39	-123.49	0.69	0.16	0.78	0.27	1.1	0.9
PGC5	48.65	-123.45	0.77	0.21	0.05	0.45	1.80	1.0
NANO	49.29	-124.08	2.23	0.27	1.77	0.36	2.50	0.90
UCLU	48.92	-125.54	2.46	0.23	1.89	0.33	2.70	0.90
DRAO	49.32	-119.62	1.01	0.21	1.15	0.34	1.20	0.70
SC02	48.55	-123.01	0.26	0.20	0.30	0.36	0.80	1.30
SEAT	47.65	-122.31	0.09	0.33	-0.21	0.31	-0.60	0.90
NEAH	48.29	-124.62	3.24	0.19	3.20	0.30	3.50	1.00
PCOL	47.17	-122.57	-0.64	0.31	-0.64	0.34		
P423	47.29	-122.94	-0.37	0.23	-0.91	0.29		
RPT1	47.39	-122.37	-1.83	0.39	NaN	NaN		
KTBW	47.55	-122.79	-0.50	0.20	-0.44	0.26		
P426	47.80	-122.51	-2.36	0.25	-2.60	4.12		
P437	48.00	-122.46	-0.42	0.29	-1.38	0.66		
BLYN	48.02	-122.93	1.85	1.53	-2.92	2.43		
P435	48.06	-123.50	0.59	0.37	0.10	0.35		
COUP	48.22	-122.68	-1.05	0.33	1.10	2.59		
WHD1	48.31	-122.69	-0.53	0.84	NaN	NaN		
P439	48.71	-122.91	-0.01	0.23	-0.29	0.41		
SC04	48.92	-123.70	1.23	0.19	1.03	0.22		
PTAL	49.26	-124.86	3.48	0.14	0.04	0.55		
GLDR	49.68	-126.13	4.01	0.53	3.02	0.57		
ELIZ	49.87	-127.13	2.46	0.22	2.57	0.35		
QUAD	50.13	-125.33	4.34	0.35	3.85	0.44		
WOST	50.21	-126.60	5.31	2.35	NaN	NaN		
BCOV	50.54	-126.84	2.76	0.19	3.55	0.65		
HOLB	50.64	-128.13	2.39	0.21	0.87	0.98		
P161	40.64	-124.21	-0.95	0.24	-1.47	0.34		
P159	40.50	-124.28	-0.83	0.25	-1.58	0.28		
P162	40.69	-124.24	-1.22	0.24	-1.59	0.29		

TRND	41.05 -124.15	-0.85	0.27	-0.70	0.28	
P316	41.56 -124.08	-2.18	0.53	-2.06	0.59	
PTSG	41.78 -124.25	3.56	0.23	3.03	0.25	
P734	42.07 -124.29	3.17	0.28	2.03	0.36	
P362	42.21 -124.23	2.79	0.34	2.05	0.41	
P733	42.44 -124.41	2.47	0.29	0.89	0.33	
CABL	42.84 -124.56	1.21	0.22	1.43	0.24	
P364	43.09 -124.41	2.32	0.29	1.73	0.44	
P365	43.39 -124.25	0.99	0.27	0.01	0.40	
P366	43.61 -123.98	0.67	0.34	-0.60	0.34	
P367	44.59 -124.06	-0.22	0.34	-0.81	0.39	
P395	45.02 -123.86	0.17	0.35	-0.15	0.34	
P396	45.31 -123.82	1.06	0.45	0.16	0.41	
CHZZ	45.48 -123.98	0.19	0.38	0.81	0.24	
TPW2	46.21 -123.77	0.23	0.16	0.48	0.22	
P398	46.92 -123.92	1.45	0.27	0.55	0.41	
PABH	47.21 -124.20	0.22	0.19	0.23	0.30	
P402	47.77 -124.31	2.47	0.24	1.66	0.45	
PTRF	48.54 -124.41	4.99	0.65	1.66	1.01	
BAMF	48.84 -125.13	2.69	0.42	1.76	0.44	
TFNO	49.15 -125.91	2.86	0.53	1.47	0.46	
NTKA	49.59 -126.62	3.58	0.24	4.27	0.44	

Estimated relative sea-level rise (RSLR) around Pacific Northwest at selected stations. Note for each noise model (ARMA(p,q), ARFIMA(p,d,q), GGM), the optimum lags p and q are selected either by minimizing the AIC or BIC (*Burnham and Anderson, 2002*). Our results are compared with previous studies (*Douglas, 1991; Mazzotti et al., 2007; Wöppelmann et al., 2009; Sweet et al., 2014; NRC, 2015*). μ is the estimated RSLR with σ the associated uncertainty. Uncertainties are one sigma. *Montillet et al. (2018)*

Source	Tide Gauge	Period (date/yr)	Rate SLR mm/yr	
			μ	σ
<i>Douglas (1991)</i>	Friday H., WA	1930-1980	0.6	N/A
<i>Mazzotti et al. (2007)</i>	Friday H., WA	62 yr	0.9	0.3
<i>Sweet et al. (2014)</i>	Friday H., WA	1934-2006	1.13	0.33
<i>NRC (2015)</i>	Friday H., WA	1934-2008	1.04	N/A
<i>Our Study</i>	Friday H., WA	1934-2014		
(AIC) ARMA(4,0)			1.07	0.18
(AIC) ARFIMA(3,-0.50± 0.11,0)			1.05	0.09
(AIC) GGM			1.07	0.19
(BIC) ARMA(1,1)			1.07	0.18
(BIC) ARFIMA(1,-0.65± 0.06,1)			1.05	0.08
(BIC) GGM			1.07	0.19
<i>Douglas (1991)</i>	Neah Bay, WA	1930-1980	-1.6	N/A
<i>Mazzotti et al. (2007)</i>	Neah Bay, WA	44 yr	-1.6	0.6
<i>Wöppelmann et al. (2009)</i>	Neah Bay, WA	65 yr	-1.59	0.22
<i>Sweet et al. (2014)</i>	Neah Bay, WA	1934-2006	-1.63	0.36
<i>NRC (2015)</i>	Neah Bay, WA	1934-2008	-1.77	N/A
<i>Our Study</i>	Neah Bay, WA	1934-2014		
(AIC) ARMA(3,0)			-1.76	0.19
(AIC) ARFIMA(1,-0.65± 0.12,2)			-1.79	0.10
(AIC) GGM			-1.76	0.21
(BIC) ARMA(1,1)			-1.76	0.19
(BIC) ARFIMA(1,0.17± 0.05,0)			-1.74	0.30
(BIC) GGM			-1.76	0.21
<i>Douglas (1991)</i>	Seattle, WA	1930-1980	2.50	N/A
<i>Mazzotti et al. (2007)</i>	Seattle, WA	92 yr	2.20	0.20
<i>Wöppelmann et al. (2009)</i>	Seattle, WA	104 yr	2.06	0.11
<i>Sweet et al. (2014)</i>	Seattle, WA	1898-2006	2.06	0.17
<i>NRC (2015)</i>	Seattle, WA	1934-2008	2.01	N/A
<i>Our Study</i>	Seattle, WA	1934-2014		
(AIC) ARMA(1,2)			2.01	0.11
(AIC) ARFIMA(0,0.15± 0.04,4)			1.97	0.15
(AIC) GGM			2.01	0.19
(BIC) ARMA(1,1)			2.00	0.10
(BIC) ARFIMA(1,0.24± 0.04,0)			1.96	0.20
(BIC) GGM			2.01	0.19
<i>Douglas (1991)</i>	Astoria, OR	1930-1980	-0.40	N/A
<i>Mazzotti et al. (2007)</i>	Astoria, OR	77 yr	-0.40	0.30
<i>Sweet et al. (2014)</i>	Astoria, OR	1925-2006	-0.31	0.40
<i>NRC (2015)</i>	Astoria, OR	1925-2008	-0.38	N/A
<i>Our Study</i>	Astoria, OR	1925-2014		
(AIC) ARMA(3,3)			-0.26	0.22

(AIC) ARFIMA(3,0.09± 0.12,0)			-0.31	0.11
(AIC) GGM			-0.25	0.24
(BIC) ARMA(1,0)			-0.26	0.21
(BIC) ARFIMA(0,0.27± 0.04,1)			-0.22	0.40
(BIC) GGM			-0.25	0.24
Douglas (1991)	Crescent, CA	1930-1980	-0.9	N/A
Sweet et al. (2014)	Crescent, CA	1933-2006	-0.65	0.36
NRC (2015)	Crescent, CA	1933-2008	-0.73	N/A
Our Study	Crescent, CA	1933-2014		
(AIC) ARMA(4,0)			-0.81	0.19
(AIC) ARFIMA(3,-0.59± 0.11,0)			-0.80	0.10
(AIC) GGM			-0.81	0.20
(BIC) ARMA(1,0)			-0.82	0.16
(BIC) ARFIMA(1,0.19± 0.06,0)			-0.77	0.30
(BIC) GGM			-0.81	0.20

Table 8: Estimation of the Relative SL (RSL) rise and corrected RSL rise with interpolated GPS uplift velocities. Uncertainties (grey) are one sigma. The field ID refers to the numbers labeling the tide gauges in Figure 4 . All rates and uncertainties are in mm/yr. *Montillet et al. (2018)*

#	Tide Gauge	Lat.	Long.	Period (date/yr)	(BIC)RSLR ARMA		(BIC)RSLR ARFIMA		(BIC)RSLR GGM		VLM (Interpolated)		ASLR (ARMA)		ASLR (ARFIMA)		ASLR (GGM)	
					μ	σ	μ	σ	μ	σ	μ	σ	μ	σ	μ	σ	μ	σ
18	Campbell R., BC	50.02	-125.23	1958-2015	-1.81	0.48	-1.84	0.33	-1.81	0.53	3.52	0.29	1.71	0.40	1.68	0.31	1.71	0.43
17	P. Alberni, BC	49.23	-124.82	1947-1997	-0.62	0.58	-0.66	0.87	-0.64	0.74	3.31	0.14	2.69	0.42	2.65	0.62	2.67	0.53
16	Tofino, BC	49.15	-125.91	1909-2015	-1.08	0.38	-1.15	0.24	-1.10	0.13	2.86	0.50	1.78	0.44	1.71	0.39	1.76	0.36
15	Bamfield, BC	48.85	-125.13	1969-2015	-0.28	0.43	-0.2	0.74	-0.27	0.53	2.69	0.38	2.41	0.41	2.49	0.59	2.42	0.46
14	Patricia B., BC	48.65	-123.45	1966-2015	0.52	0.78	0.76	1.11	0.52	0.78	0.68	0.21	1.20	0.57	1.44	0.80	1.20	0.57
13	P. Renfrew, BC	48.55	-124.42	1957-1997	0.83	1.22	0.01	1.7	0.01	1.53	4.82	0.63	5.65	0.97	4.83	1.28	4.83	1.17
12	Friday Har., WA	48.55	-123.01	1934-2014	1.07	0.18	1.05	0.07	1.07	0.19	0.30	0.20	1.37	0.19	1.35	0.15	1.37	0.19
11	Victoria, BC	48.41	-123.36	1909-2015	0.7	0.13	0.74	0.06	0.7	0.14	0.64	0.36	1.34	0.27	1.38	0.26	1.34	0.27
10	P. Townsend, WA	48.11	-122.76	1972-2015	1.67	0.52	1.76	0.76	1.71	0.57	0.06	0.36	1.73	0.44	1.82	0.59	1.77	0.48
09	Ncah Bay, WA	48.36	-124.61	1930-1980	-1.76	0.19	-1.74	0.30	-1.76	0.21	3.68	0.31	1.92	0.26	1.94	0.30	1.92	0.26
08	P. Angeles, WA	48.12	-123.44	1975-2015	-0.06	0.51	0.15	0.87	0.01	0.66	-0.04	0.36	-0.10	0.44	0.11	0.67	-0.03	0.53
07	Seattle, WA	47.60	-122.33	1934-2014	2.00	0.10	1.96	0.20	2.01	0.12	-0.12	0.28	1.88	0.21	1.84	0.24	1.89	0.21
06	Astoria, OR	46.21	-123.77	1925-2014	-0.26	0.21	-0.22	0.40	-0.25	0.24	0.28	0.18	0.02	0.20	0.06	0.31	0.03	0.21
05	South Beach, OR	44.62	-124.04	1967-2014	2.25	0.50	2.28	0.72	2.27	0.56	-0.19	0.34	2.06	0.42	2.09	0.56	2.08	0.46
04	Charleston II, OR	43.34	-124.32	1970-2015	0.88	0.53	0.96	0.73	0.86	0.53	1.23	0.28	2.11	0.42	2.19	0.55	2.09	0.42
03	P. Orford, OR	42.74	-124.49	1985-2015	0.94	0.83	1.38	1.35	1.06	0.97	1.52	0.24	2.46	0.61	2.90	0.97	2.58	0.71
02	Crescent, CA	41.74	-124.18	1933-2014	-0.83	0.16	-0.77	0.30	-0.80	0.20	2.46	0.29	1.63	0.23	1.69	0.29	1.66	0.25
01	Humboldt, CA	40.76	-124.22	1985-2015	5.06	0.92	5.63	1.48	5.19	1.02	-1.15	0.22	3.91	0.67	4.48	1.05	4.04	0.74